Rapid allylic 1,6 H-atom transfer in an unsaturated Criegee intermediate

Anne S. Hansen¹, Yujie Qian¹, Christopher A. Sojdak¹, Marisa C. Kozlowski¹, Vincent J. Esposito¹, Joseph S. Francisco¹, Stephen J. Klippenstein²*, and Marsha I. Lester¹*

¹Department of Chemistry, University of Pennsylvania, Philadelphia, PA 19104-6323 USA ²Chemical Sciences and Engineering Division, Argonne National Laboratory, Lemont, IL 60439 USA

<u>Abstract</u>

A novel allylic 1,6 hydrogen atom transfer mechanism is established through infrared activation of the 2-butenal oxide Criegee intermediate, resulting in very rapid unimolecular decay to hydroxyl (OH) radical products. A new precursor, Z/E-1,3-diiodobut-1-ene, is synthesized and photolyzed in the presence of oxygen to generate a new four-carbon Criegee intermediate with extended conjugation across the vinyl and carbonyl oxide groups that facilitates rapid allylic 1,6 H-atom transfer. A low-energy reaction pathway involving isomerization of 2-butenal oxide from a lower energy (tZZ) conformer to a higher energy (cZZ) conformer followed by 1,6 hydrogen transfer via a 7-membered ring transition state is predicted theoretically and shown experimentally to yield OH products. The low-lying (tZZ) conformer of 2-butenal oxide is identified based on computed anharmonic frequencies and intensities of its eight conformers. Experimental IR action spectra recorded in the fundamental CH stretch region with OH product detection by UV laser-induced fluorescence reveal a distinctive IR transition of the low-lying (tZZ) conformer at 2996 cm⁻¹ that results in rapid unimolecular decay to OH products. Statistical RRKM calculations involving a combination of conformational isomerization and unimolecular decay via 1,6 H-transfer yield an effective decay rate $k_{\text{eff}}(E)$ on the order of 10⁸ s⁻¹ at ca. 3000 cm⁻¹ in good accord with experiment. Unimolecular decay proceeds with significant enhancement due to quantum mechanical tunneling. A rapid thermal decay rate of ca. 10⁶ s⁻¹ is predicted by master-equation modeling of 2-butenal oxide at 298 K, 1 bar. This novel unimolecular decay pathway is expected to increase the non-photolytic production of OH radicals upon alkene ozonolysis in the troposphere.

1

^{*)} Corresponding authors: milester@sas.upenn.edu; sjk@anl.gov

1. Introduction

Alkenes are an abundant component of the volatile organic compounds emitted into the atmosphere, second only to methane, and originate from both biogenic and anthropogenic sources.¹ Ozonolysis is a major atmospheric removal pathway for alkenes.²⁻⁶ Alkene ozonolysis proceeds by cycloaddition of ozone across a carbon-carbon double bond to form a primary ozonide (POZ), which then decomposes to form carbonyl and zwitterionic carbonyl oxide (R₁R₂CO⁺O⁻) products.⁷⁻⁸ The latter is known as the Criegee intermediate. The orientation of the carbonyl oxide group relative to substituents (R₁, R₂) leads to two classes of conformers, *syn* and *anti*, for asymmetrically substituted Criegee intermediates. Significant barriers generally restrict interconversion between the *syn* and *anti* conformers.⁹⁻¹⁰

Unimolecular decay of Criegee intermediates is a significant source of OH radicals in the troposphere, contributing up to 1/3 of the OH radicals in the daytime and essentially all of the OH radicals at nighttime.^{2,5-6} Unimolecular decay pathways for Criegee intermediates are highly substituent (R₁, R₂) and conformer dependent.⁹ *Syn* conformers that have an alkyl substituent adjacent to the carbonyl oxide group can undergo unimolecular decay *via* an alkyl 1,4 H-atom transfer mechanism to form OH radical products. This unimolecular decay pathway proceeds by α -H-atom transfer to the terminal oxygen *via* a 5-membered ring transition state (TS) to form a vinyl hydroperoxide (VHP), as shown in Scheme 1 (top). VHP then decomposes to produce OH and a vinoxy radical products.¹⁰⁻¹⁵

Alkyl 1,4 H-shift

$$R
ightharpoonup O
ightharpoonup O$$

Scheme 1: Illustration of the alkyl 1,4 H-atom (top) and allylic 1,6 H-atom (bottom) transfer mechanisms for unimolecular decay of Criegee intermediates with a *syn*-alkyl H-atom.

This group has studied the 1,4 H-atom transfer mechanism associated with unimolecular decay of several Criegee intermediates by infrared (IR) action spectroscopy with detection of OH radical products under collision free conditions. 13-14, 16-20 The Criegee intermediates are generated using an alternative synthetic method described below, ²¹⁻²² and subsequently activated via IR excitation to access energies in the vicinity of the TS barrier. This protocol imparts sufficient energy to either surmount or tunnel through the TS barrier, and initiates unimolecular decay and formation of OH radical products. For Criegee intermediates with two to four carbon atoms studied to date, the TS barriers for the 1,4 H-atom transfer vary from ca. 15.5 to 18 kcal mol⁻¹ with energy-dependent rates measured in the overtone CH stretch (2v_{CH}) region (ca. 6000 cm⁻¹) ranging from 2.6×10^8 to 1.8×10^6 s⁻¹. ^{16-20, 23} Excellent agreement has been found between experimentally measured and calculated Rice-Ramsperger-Kassel-Marcus (RRKM) rates, validating the calculated high-level theoretical TS barriers, the importance of quantum mechanical tunneling in the 1,4 H-atom transfer process, as well as the appropriateness of the tunneling corrected statistical RRKM framework. Thus far, 1,4 H-atom transfer^{10, 15} and CH₂OO dissociation²⁴ mechanisms have been investigated experimentally for OH production from Criegee intermediates.

The presence of an unsaturated carbon substituent adjacent to the carbonyl oxide group can have a stabilizing effect on the reactant, TS, and the resulting products. In addition, if the substituent adjacent to the carbonyl oxide group is CH=CHCH₃, as shown in Scheme 1 (bottom), theoretical calculations suggest that the Criegee intermediate may undergo an allylic 1,6 H-atom transfer process.^{9,25} In this case, the TS will have a 7-membered ring structure with reduced ring strain, which is predicted to significantly lower the TS barrier (by ca. 7 kcal mol⁻¹).⁹ It is well established for many systems, e.g. peroxy and alkoxy radicals,²⁶⁻³⁰ that ring strain at the transition state affects the magnitude of the barrier and can lead to significant changes in the rate of H-transfer reactions. Here, we demonstrate for the first time the significant reduction in the TS barrier and enhancement in rate for 1,6 H-atom transfer and unimolecular decay of a Criegee intermediate.

In this study, we investigate the allylic 1,6 H-atom transfer mechanism of the 2-butenal oxide Criegee intermediate [CH₃CH=CHCHOO, R=H in Scheme 1 (bottom)]. 2-butenal oxide can be formed upon ozonolysis of 1,3-pentadiene (see supporting information, SI, Scheme S1) and other branched unsaturated and asymmetric alkenes. 1,3-Pentadiene is a representative diolefin

analogous to 1,3-butadiene and isoprene. The OH yield from ozonolysis of 1,3-pentadiene has previously been measured to be ca. 0.8, which is larger than those measured for 1,3-butadiene and isoprene due to the additional methyl group and the location of that group, respectively.³¹

The 2-butenal oxide Criegee intermediate is predicted to have eight conformers: four syn (Z) and four anti (E) conformers with the syn and anti conformers connected via significant torsional barriers restricting interconversion between them; see Tables S1 – S3. 9,32 The four syn conformers of 2-butenal oxide that can potentially generate OH radical products, cis-Z-(Z-CH=CHCH₃)CHOO (cZZ), trans-Z-(Z-CH=CHCH₃)CHOO (tZZ), trans-Z-(E-CH=CHCH₃)CHOO (tZE), and cis-Z-(E-CH=CHCH₃)CHOO (cZE), are shown in Figure 1. The first Z in the notation refers to the orientation of the carbonyl oxide group. The second Z, or alternatively E, refers to the orientation of the vinyl group. The tZZ and tZE conformers are connected by internal rotation about the vinyl group via a high barrier that restricts interconversion. Internal rotation about the C-C single bond connects cis and trans conformers (formally s-cis and s-trans, but simplified herein as cis and trans) via low barriers. Only the cZZ conformer can undergo the allylic 1,6 H-atom transfer process. However, the tZZ conformer can isomerize to cZZ (barrier of 8.2 kcal mol⁻¹) and thereby contribute to the hydrogen transfer process. The tZZ, tZE, and cZE conformers can undergo a vinyl H-atom transfer process, which can potentially lead to the formation of OH radical products. However, the TS barriers for these vinyl hydrogen transfer mechanisms are high (>25 kcal mol⁻¹)^{9, 16} and energetically inaccessible in the present study; see SI for additional details. The cZE and tZE conformers may also decay via an alternative 1,5-ring closure pathway to dioxole (Scheme S4) that is not expected to yield OH products. 9, 16, 33-34 The high interconversion barriers indicate that only two conformers, tZZ and cZZ, are relevant for IR activated unimolecular decay to OH radical products under jetcooled conditions.

Herein, we investigate the IR action spectrum of the 2-butenal oxide Criegee intermediate and its energy-dependent unimolecular decay rate. Upon IR activation, a low-energy conformer (*tZZ*, 2.0 kcal mol⁻¹) of 2-butenal oxide isomerizes to a higher energy conformer (*cZZ*, 6.2 kcal mol⁻¹), which undergoes the allylic 1,6 H-atom transfer and release of OH radical products that are detected. The present study provides the first experimental demonstration of very fast allylic 1,6 H-atom transfer and unimolecular decay in a Criegee intermediate, which had been predicted theoretically.⁹

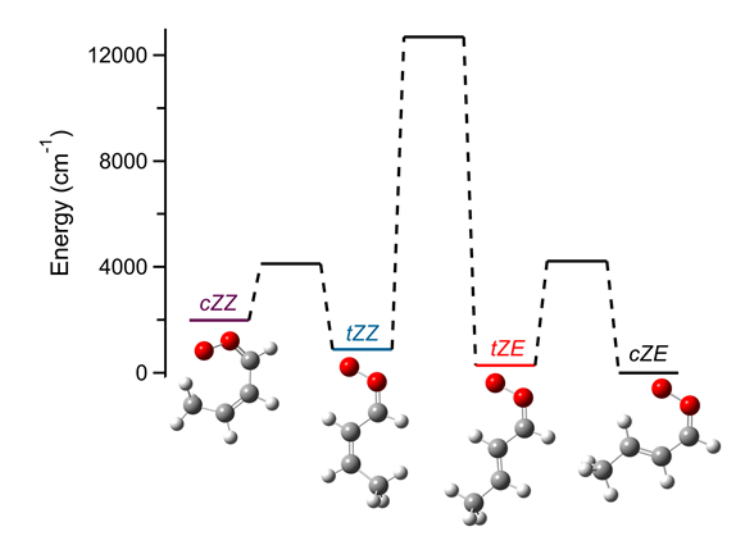


Figure 1: Interconversion barriers for *syn* conformers of the 2-butenal oxide Criegee intermediate. Low barriers connect the *cis* (*c*) and *trans* (*t*) conformers (for example, *cZZ* and *tZZ*) *via* internal rotation about a single C-C bond. A high barrier of ca. 12000 cm⁻¹ connects the *tZZ* and *tZE* conformers *via* internal rotation about the double C=C bond. All energies are calculated at the B2PLYP-D3/cc-pVTZ level of theory and include anharmonic zero-point energy correction.

2. Methods

2.1 Synthesis

Previously H- or alkyl-substituted Criegee intermediates [CH₂OO,^{21, 35} CH₃CHOO,^{22, 36-37} (CH₃)₂COO,³⁸⁻³⁹ CH₃CH₂CHOO,²⁶ and (CH₃)(CH₃CH₂)COO (MECI)^{20, 40}] have been generated by photolysis of *gem*-diiodoalkane precursors, which form a monoiodoalkyl radical that subsequently reacts with O₂ to form the Criegee intermediate (Scheme S2). For unsaturated four carbon Criegee intermediates derived from isoprene ozonolysis [methyl vinyl ketone oxide (MVK-oxide)^{16, 41} and methacrolein oxide (MACR-oxide)³³], a modified synthetic approach has been developed that relies upon a 1,3-iodoallylic iodide precursor. These compounds are excellent precursors to Criegee intermediates owing to the lability of the C–I bond, which allows facile radical generation as well as facile elimination upon trapping of O₂ (see Scheme S2).

In this work, a new precursor, (Z/E)-1,3-diiodobut-1-ene [CH(I)=CHCH(I)CH₃], is synthesized to generate the 2-butenal oxide Criegee intermediate for the first time. However, the very reactivity, which includes light and thermal sensitivity, that renders these compounds suitable as Criegee precursors complicates their generation, handling, and storage. The reported approach to analogs of this precursor involves an intramolecular rearrangement of propargyl

alcohols with trimethylsilyl iodide; $^{42-43}$ however, three issues arise with these methods when applied to this target. One issue is the high reactivity of trimethylsilyl iodide, which can cause formation of numerous byproducts. Another is the lack of reactivity as well as selectivity with the use of secondary alcohols relative to the reported primary alcohols. Finally, this approach is unable to produce the desired 1,3-iodoallylic iodides when terminal alkynes are used. On account of these pitfalls, a new approach was proposed to allow access to a broader range of 1,3-iodoallylic iodides in higher yields. Specifically, installation of the two iodo groups in separate steps would prevent rearrangements or addition of iodine to the incorrect position, which is often observed in the synchronous installation of both iodo groups. Thus, the vinyliodide was first generated by conjugate addition of iodide and subsequent DIBAL-H reduction of the ester, 44 to yield the two alkene isomers of 1,3-iodoallylic alcohol. The hydroxyl group was then displaced with iodide using a very mild Appel reaction to generate (Z/E)-1,3-diiodobut-1-ene in 39% overall yield. The greater selectivity and high yield of this approach is expected to facilitate access to a range of Criegee precursors. An overview of the synthesis is shown in Scheme 2; further details are provided in the SI (Figures S1 – S6).

OMe
$$\frac{a}{85\%}$$
 OMe $\frac{b}{71\%}$ OH $\frac{c}{64\%}$ $\frac{c}{64\%}$ $(Z):(E)=0.69:0.31$ $(Z):(E)=0.45:0.55$

Scheme 2: *a*) NaI (1.6 equiv), AcOH 120 °C, 2 h. *b*) DIBAL-H (1 equiv), MeMgBr (1.5 equiv), CH₂Cl₂, −78 °C→rt, 2 h. *c*) PPh₃ (1.4 equiv), 1H-Imidazole (1.4 equiv), I₂ (1.4 equiv), CH₂Cl₂, rt, 1h.

Photolysis of (Z/E)-1,3-diiodobut-1-ene at 248 nm results in preferential dissociation of the weaker allylic C-I bond (sp3-hybridized), rather than the vinyl C-I bond; see Scheme S2. The resultant allylic monoiodoalkene radical is resonance stabilized, enabling the radical center initially formed on the primary carbon to shift to a more stable secondary carbon site. Addition of O_2 at the radical site forms an energized iodoalkene radical, and the subsequent loss of an iodine atom leads to formation of 2-butenal oxide in up to eight conformational forms.

2.2 Spectroscopic Methods

The (Z/E)-1,3-diiodobut-1-ene precursor is heated to 50°C, entrained in a 20% O₂/Ar carrier gas (30 psi), and pulsed through a 1 mm ID quartz capillary reactor tube (25 mm length) where it is photolyzed near the tip using the focused 248 nm output from a KrF excimer laser (Coherent

COMPex Pro 50F; ca. 5 mJ pulse⁻¹, 10 Hz). Subsequent reaction with O₂ generates the 2-butenal oxide Criegee intermediate, which is collisionally stabilized in the capillary and cooled under supersonic jet expansion to a rotational temperature of ca. 10 K.¹³⁻¹⁴ The 2-butenal oxide Criegee intermediate is initially detected by photoionization using 10.5 eV vacuum ultraviolet (VUV) radiation on the parent m/z = 86 mass channel using a time-of-flight mass spectrometer as shown in Figure S7 and described in the SI.

Most experiments utilized an IR pump-UV probe scheme to obtain IR action spectra and time-dependent unimolecular decay rates. As described in previous studies, ^{13-14, 16-17} tunable IR radiation from an optical parametric oscillator/amplifier (OPO/OPA, Laservision) pumped by an unseeded Nd:YAG laser (1064 nm, Continuum Surelite EX) is overlapped with UV radiation from a Nd:YAG pumped dye laser (Ekspla NL303HT, Continuum ND6000) approximately 1 cm downstream from the tip of capillary. The overlapping IR and UV beams intersect the expanding gas mixture containing cooled and stabilized 2-butenal oxide in the collision-free region. Tunable IR radiation excites 2-butenal oxide in the fundamental CH stretch (v_{CH}) region, inducing unimolecular decay, and the resultant OH $X^2\Pi_{3/2}$ products are detected by UV laserinduced fluorescence (LIF) on the A-X (1,0) $Q_1(3.5)$ transition. Two types of experiments are performed: (1) The IR pump laser is scanned with the IR-UV time delay fixed at 40 ns. (2) The IR-UV time delay is stepped to measure the time-dependent appearance of OH products upon IR activation of 2-butenal oxide (Figures S8 – S9). Because OH products can also arise from unimolecular decay of energized 2-butenal oxide in the capillary and subsequent jet-cooling, an active OH background subtraction scheme is utilized (IR on – IR off) to obtain the IR-induced signal.

2.3 Theoretical Methods

The energies of the 2-butenal oxide conformers, TS barriers, torsional barriers and products relevant for production of OH radical products *via* the 1,6 H-atom transfer process are characterized by electronic structure calculations performed at the ANL0-B2F level of theory [CCSD(T)-F12b/CBS(TZ-F12,QZ-F12)//B2PLYP-D3-BJ/cc-pVTZ + post-CCSD(T) and other corrections], as described previously, ^{16, 45} and detailed in the SI. The ANL0-B2F method is performed for the lowest energy conformer of 2-butenal oxide and those relevant to the 1,6 H-atom transfer mechanism, while the other conformers are computed at the CCSD(T)-F12/cc-pVTZ-F12//B2PLYP-D3-BJ/cc-pVTZ level of theory; see Tables S1 – S2. Hereafter, B2PLYP-

D3-BJ is abbreviated as B2PLYP-D3.⁴⁶ The majority of the coupled cluster calculations are performed with Molpro, ⁴⁷⁻⁴⁸ while a few additional electronic corrections are obtained with CFOUR, ⁴⁹⁻⁵⁰ and vibrational corrections are obtained with Gaussian16.⁵¹ Torsional barriers connecting different conformers are either obtained from torsional scans or single point energy optimizations with the B2PLYP-D3/cc-pVTZ method (Table S3). The torsional barrier connecting the *tZZ* and *cZZ* conformers are also calculated with the ANL0-B2F method. IR absorption spectra in the v_{CH} region are calculated at the B2PLYP-D3/cc-pVTZ level of theory using hybrid, degeneracy-corrected, second-order vibrational perturbation theory (HDCVPT2), ⁵²⁻⁵⁴ hereafter denoted as VPT2, as implemented in Gaussian16⁵¹ utilizing XSEDE resources. ⁵⁵

The energy-dependent unimolecular decay rates are calculated utilizing statistical RRKM theory. Solver Quantum mechanical tunneling is included using the one-dimensional Eckart model as implemented in Master Equation System Solver (MESS). Low frequency vibrations are treated as torsional motions; see SI for additional details. Master equation modeling has also been utilized to extend the energy-dependent unimolecular decay rates $k_{\text{eff}}(E)$ for 2-butenal oxide to thermal conditions $k_{\text{eff}}(T, P)$ using MESS; see SI for additional details.

3. Results

3.1 Calculated Conformational Barriers and Reaction Energy Profile

Figure 2a shows the energy profile computed for the unimolecular decay of 2-butenal oxide to OH products. Although the energies of the eight conformers are shown, including the lowest energy *cis-Z-(E-CH=CHCH*₃)CHOO conformer (*cZE*, black; 0.0 kcal mol⁻¹), only two conformers are relevant in the present study: *tZZ* (blue; 2.0 kcal mol⁻¹) and *cZZ* (purple; 6.2 kcal mol⁻¹). The *tZZ* conformer can isomerize to the *cZZ* conformer, from which unimolecular decay can occur *via* an allylic 1,6 H-atom transfer mechanism through a 7-membered ring TS to produce (*E*)-1-hydroperoxybuta-1,3-diene (HPBD, CH₂=CHCH=CHOOH), followed by decomposition to OH and 1-oxobut-3-enyl (CH₂=CH•CHCHO) radical products. The TS barrier associated with allylic 1,6 H-atom transfer lies 9.1 kcal mol⁻¹ (ca. 3190 cm⁻¹) higher than *tZZ* and 4.9 kcal mol⁻¹ (ca. 1710 cm⁻¹) greater than *cZZ*. The isomerization from *tZZ* to the higher energy *cZZ* conformer occurs *via* a torsional barrier of 8.2 kcal mol⁻¹ (ca. 2860 cm⁻¹, relative to *tZZ*) associated with internal rotation about the C-C bond (Figure 2b). The energy required to

isomerize from *tZZ* to *cZZ* is predicted to be close to, but not above, the TS barrier leading to OH radical products. The other *syn* and *anti* conformers of 2-butenal oxide, including the lowest energy *cZE* conformer, are separated from the *tZZ* and *cZZ* conformers by very high barriers (involving internal rotation about C=O or C=C bonds, Table S3), precluding interconversion to the *tZZ* and *cZZ* conformers upon IR activation at ca. 3000 cm⁻¹.

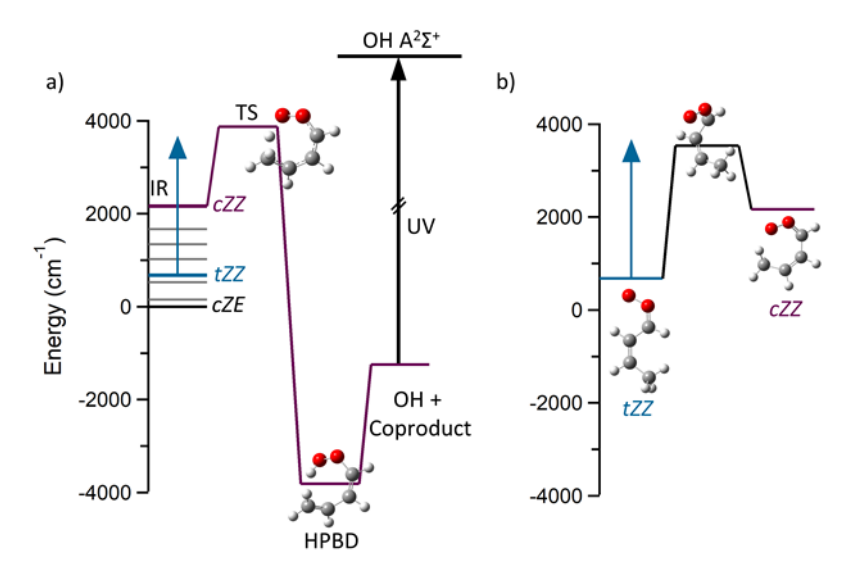


Figure 2: a) Energy profile for unimolecular decay of 2-butenal oxide to OH radical products. Energies are given relative to the lowest energy *cis-ZE*-2-butenal oxide (*cZE*, black) conformer. Energies for the eight conformers of 2-butenal oxide (Figure S10) are shown, although only *cis-ZZ*-2-butenal oxide (*cZZ*, purple) can undergo the allylic 1,6-hydrogen transfer leading to (*E*)-1-hydroperoxybuta-1,3-diene (HPBD) and followed by rapid decomposition to OH and OCH₂CHCH radical products. Unimolecular decay is initiated by IR activation of *trans-ZZ*-2-butenal oxide (*tZZ*, blue) that can isomerize to *cZZ via* a torsional barrier of 2860 cm⁻¹. b) The interconversion barrier between the *tZZ* and *cZZ* conformers of 2-butenal oxide. All energies include anharmonic zero-point correction. Energies for *tZZ*, *cZZ*, and the stationary points along the reaction pathways for unimolecular H-atom transfer and isomerization are calculated with the ANL0-B2F method, while energies for other 2-butenal oxide conformers are computed with the CCSD(T)-F12/cc-pVTZ-F12//B2PLYP-D3/cc-pVTZ method; see Tables S1 – S2.

3.2 Calculated IR Absorption and Observed IR-Action Spectra

The experimental search to identify IR transitions of jet-cooled (rotational temperature $T_{\rm rot}$ ~10 K) and stabilized 2-butenal oxide in the $v_{\rm CH}$ region is guided by anharmonic frequency calculations obtained using VPT2 calculations. We anticipate that multiple low-energy conformers of 2-butenal oxide will be populated under the present experimental conditions, as found for simpler Criegee intermediates^{20, 58} and alkyl benzenes⁵⁹⁻⁶¹ investigated through infrared excitation under jet-cooled conditions. Here, we focus on two conformers, tZZ and cZZ, which

are relevant to the low-energy unimolecular decay pathway leading to OH radical products. The lower energy tZZ conformer (2.0 kcal mol⁻¹) is expected to be significantly more populated than cZZ (6.2 kcal mol⁻¹). Thus, we focus on the reaction pathway:

$$tZZ \longrightarrow cZZ \longrightarrow OH + co-products$$

IR activation of the tZZ conformer with one quantum of CH stretch ($v_{CH} \sim 3000 \text{ cm}^{-1}$) provides sufficient energy to overcome the torsional barrier, thereby accessing the higher energy cZZ conformer, which in turn can undergo 1,6 H-transfer and unimolecular decay OH products.

The anharmonic calculated absorption IR spectrum for the tZZ conformer in the fundamental CH stretch region (2900 – 3150 cm⁻¹) is shown in Figure 3a and 3b. The calculated IR spectra for the higher energy cZZ conformer is also shown in Figure 3a, while calculated spectra for tZZ, cZZ, and all other conformers are compared in Figure S11. The calculated transitions for the tZZ conformer are convoluted with a Gaussian function (full width half maximum (FWHM) of 4.5 cm⁻¹) in Figure 3b to represent the typical simulated breadth of the rotational band contour under jet-cooled conditions (Figure S12). $^{13-14}$

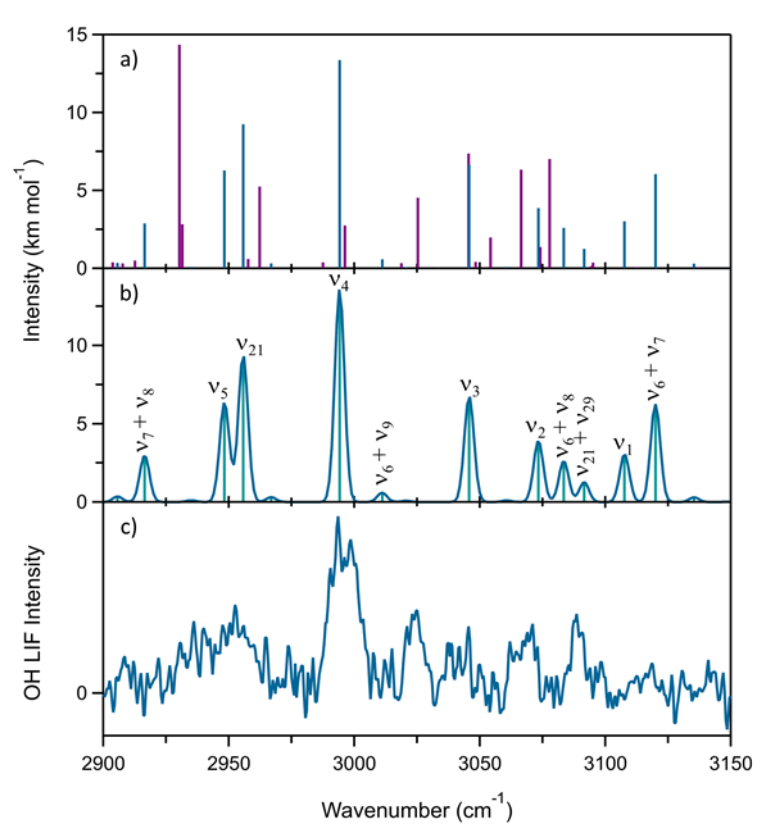


Figure 3: a) IR frequencies and intrinsic intensities (sticks) computed for the cZZ (purple) and tZZ (blue) conformers of 2-butenal oxide in the fundamental CH stretch (v_{CH}) region using VPT2 at the B2PLYP-D3/cc-pVTZ level of theory; see Tables S4 – S6. b) broadened IR spectrum

predicted for the tZZ conformer of 2-butenal oxide obtained by convoluting the stick spectrum with a Gaussian function (FWHM ~4.5 cm⁻¹) representing the typical breadth of a rotational band contour for isolated vibrational transitions under jet-cooled conditions (see Figure S12). Spectral labels are defined in Tables S4 – S5; only transitions with intensities >0.5 km mol⁻¹ are labeled. c) Experimental IR action spectrum attributed to the tZZ conformer of 2-butenal oxide obtained with UV LIF detection of OH products at an IR-UV time delay of 40 ns.

The calculated spectrum for the tZZ conformer in the $2900-3150~\rm cm^{-1}$ region consists of sixteen vibrations, where six are fundamental CH stretch vibrations and ten are combination transitions involving lower frequency vibrations (Tables S4 and S5). The carbonyl oxide CH stretch is predicted to have the highest fundamental CH stretch frequency (v_1 : 3108 cm⁻¹), followed by the vinyl CH stretches (v_2 : 3073 and v_3 : 3046 cm⁻¹), and finally the methyl CH stretches (v_4 : 2994, v_5 : 2948, and v_{21} : 2956 cm⁻¹), as found previously for other Criegee intermediates. Most of the CH stretches (Table S4) have A' symmetry, although one has A'' symmetry (v_{21} : 2956 cm⁻¹). The strongest computed IR transition is associated with a CH stretch of the methyl group at 2994 cm⁻¹ (A'). Combination transitions are predicted both below and above the fundamental CH stretches with the strongest of these transitions located at 3120 cm⁻¹ ($v_6 + v_7$, Table S5). Experimentally, we anticipate observing feature(s) in the IR action spectrum primarily at energies above the torsional barrier connecting tZZ and cZZ (ca. 2860 cm⁻¹); cZZ is the only conformer that can result in 1,6 H-atom transfer to OH radical products at these energies.

Figure 3c shows the experimental IR action spectrum obtained in the v_{CH} region with UV LIF detection of OH radical products on the A–X (1,0) $Q_1(3.5)$ transition at a fixed IR–UV time delay of 40 ns and a scan speed of 0.05 cm⁻¹/s. The experimental spectrum from 2900 cm⁻¹ to 3150 cm⁻¹ is an average of several scans. The strongest feature is observed at 2996 cm⁻¹ and weaker features are detected at both lower (ca. 2950 cm⁻¹) and higher (ca. 3025, 3042, 3070, and 3090 cm⁻¹) frequencies. The strongest feature at 2996 cm⁻¹ (FWHM of 13 cm⁻¹) is in close proximity (within 2 cm⁻¹) to the strongest CH stretch predicted for the tZZ conformer at 2994 cm⁻¹ (v_4) associated with the methyl group. The broader feature observed at 2950 cm⁻¹ is in very good agreement with the predicted transitions for the tZZ conformer at 2948 cm⁻¹ (v_5) and 2956 cm⁻¹ (v_{21}), and is ascribed to the methyl CH stretches. The IR spectral features observed beyond 3000 cm⁻¹ are less distinctive and likely arise from the series of overlapping transitions predicted from 3046 cm⁻¹ (v_3) to 3120 cm⁻¹ ($v_6 + v_7$) for the tZZ conformer. The spectral features observed in the experimental IR action spectrum are not consistent with IR transitions computed for the

cZZ conformer as shown in Figure 3a. The cZZ conformer is predicted to have its strongest transition at 2930 cm⁻¹, where no significant IR-induced signal is observed (Table S6). This confirms our assumption of minimal initial population of the higher energy cZZ conformer.

Other conformers of 2-butenal oxide are not expected to contribute to the IR action spectrum obtained in the v_{CH} region with OH product detection. Other *syn* conformers (*cZE* and *tZE*) shown in Figure 4 are separated by a high barrier (ca. 35 kcal mol⁻¹, e.g. Figure 1) from the *cZZ* conformer, which leads to 1,6 H-atom transfer and OH products, or lack energetically accessible pathways for alternative routes to OH products (e.g. vinyl 1,4 H-atom transfer; see SI for more details). The four *anti* conformers of 2-butenal oxide (Figure S10) have high barriers (ca. 25 kcal mol⁻¹, e.g. Figure S13) separating them from *syn* conformers, again precluding their unimolecular decay to OH products.

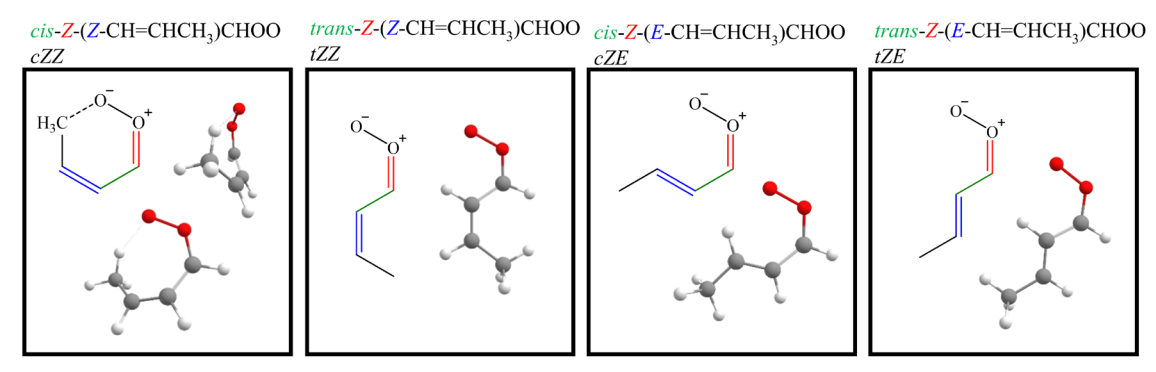


Figure 4: The four *syn*, *Z* conformers of the 2-butenal oxide Criegee intermediate with the carbonyl oxide group oriented towards the saturated carbon chain are shown with chemical structures and models. The *cis* and *trans* conformers can interconvert about the C-C bond (green, ca. 10 kcal mol⁻¹). The vinyl *Z* and *E* conformers are separated by internal rotation about the C=C bond (blue) with high barriers (ca. 35 kcal mol⁻¹). Figure S10 shows the *anti*, *E* conformers that are separated from *syn*, *Z* conformers by high barriers (ca. 25 kcal mol⁻¹) associated with internal rotation about the C=O bond (red). Tables S1 and S3 give the relative energies of the eight conformers and associated interconversion barriers.

3.3 Unimolecular Decay Rate for 1,6 H-Atom Transfer

The rate of appearance of OH products is measured following IR excitation of 2-butenal oxide at 2996 cm⁻¹, which is ascribed to the *tZZ* conformer. The OH products appear rapidly (within 5 ns) and decays on a microsecond timescale.¹⁸ The rapid rate of OH appearance is attributed to unimolecular decay involving a combination of isomerization of *tZZ* to *cZZ* and 1,6 H-atom transfer to HPBD with release of OH radicals. The decay is a purely experimental effect due to molecules moving out of the UV probe laser beam (Figure S8) and is relatively unchanged for many Criegee intermediates investigated to date.^{16-20, 58, 62-63} The temporal profile is fit with a

dual exponential function as described previously and considers the temporal resolution of the IR and UV lasers; see SI. $^{16-20, 58, 62-63}$ The rise of the temporal profile is recorded with 1 ns time steps over 40 ns and fit to evaluate k_{rise} (Figure S9). An OH appearance rate of $k_{\text{rise}} \ge 2.3 \pm 1.0 \times 10^8 \text{ s}^{-1}$ (and corresponding lifetime $\tau \le 4.4 \pm 2.0 \text{ ns}$) is obtained in the fit with $\pm 2\sigma$ uncertainty based on repeated measurements that reflects the weak signal. The value for k_{rise} is a lower limit due to the time resolution of the IR and UV lasers.

Statistical RRKM theory is also used to calculate the energy-dependent unimolecular decay rates k(E) for the tZZ and cZZ conformers of the 2-butenal oxide Criegee intermediate. Starting from the tZZ conformer of 2-butenal oxide, we consider a two-step kinetic scheme:

$$tZZ \stackrel{k_{\text{iso,f}}}{=} cZZ \stackrel{k_{\text{H-trans}}}{=} \text{product}$$

The first step involves isomerization between tZZ and cZZ with the forward (f) and reverse (r) rates (k_{iso}). The second step proceeds from the cZZ conformer to OH products via the 1,6 H-atom transfer process ($k_{H-trans}$). The overall effective rate constant can be written as:

$$k_{\text{eff}}(E) = \frac{k_{\text{H-trans}} k_{\text{iso,f}}}{k_{\text{iso,r}} + k_{\text{H-trans}}} \tag{1}$$

in which each term can be expressed as:⁵⁶

$$k(E) = \frac{\sigma_{eff}}{\sigma_{eff}^{\ddagger}} \frac{G^{\ddagger}(E - E_0)}{hN(E)}$$
 (2)

where $G^{\ddagger}(E-E_0)$ is the tunneling-weighted sum of vibrational states at the TS, N(E) is the density of vibrational states of the reactant, $\sigma_{\rm eff}$ and $\sigma_{\rm eff}^{\ddagger}$ are the effective symmetry numbers (where $\sigma_{\rm eff}$ = symmetry number / number of enantiomers) of the reactant and TS, E_0 is the TS barrier energy, and h is Planck's constant.

The effective rate in equation (1) can be simplified (see SI):

$$k_{\text{eff}}(E) = \frac{k'_{\text{H-trans}}k_{\text{iso,f}}}{k_{\text{iso,f}} + k'_{\text{H-trans}}}$$
(3)

where $k'_{\text{H-trans}}$ is a modified rate for the 1,6 H-atom transfer reaction that has been recast in terms of the density of states for the tZZ conformer (with TS of 4.9 kcal mol⁻¹, 1334i cm⁻¹, $\sigma_{\text{eff}} = 1$, and $\sigma_{\text{eff}} = 1/2$) and $k_{\text{iso,f}}$ is the rate for isomerization from tZZ to cZZ (TS barrier of 8.2 kcal mol⁻¹, 108i cm⁻¹, $\sigma_{\text{eff}} = 1$, and $\sigma_{\text{eff}} = 1/2$).

Figure 5 shows the energy dependent rates for isomerization from tZZ to cZZ ($k_{iso,f}$, green) and modified unimolecular decay from cZZ to OH products ($k'_{H-trans}$, blue), both of which include quantum mechanical tunneling via a one-dimensional Eckart model. Anharmonic vibrational frequencies are used for the reactants and the transition states except for the torsional motions, which are described as one-dimensional hindered rotors. The effective unimolecular decay rate computed at 2996 cm⁻¹ [$k_{eff}(E) = 5.6 \times 10^7 \text{ s}^{-1}$, black] is similar (within a factor of 4) to the rapid rate observed experimentally ($k_{rise} \ge 2.3 \pm 1.0 \times 10^8 \text{ s}^{-1}$). Accounting for experimental uncertainty brings the computed and experimental rates within a factor of 2. Overall, both experiment and theory reveal rapid unimolecular decay via a 1,6 H-atom transfer mechanism. These results confirm the proposed mechanism of isomerization from tZZ to cZZ followed by 1,6 H-atom transfer, along with associated barrier heights and imaginary frequencies. Potential sources of experimental and theoretical uncertainty are considered in the discussion section.

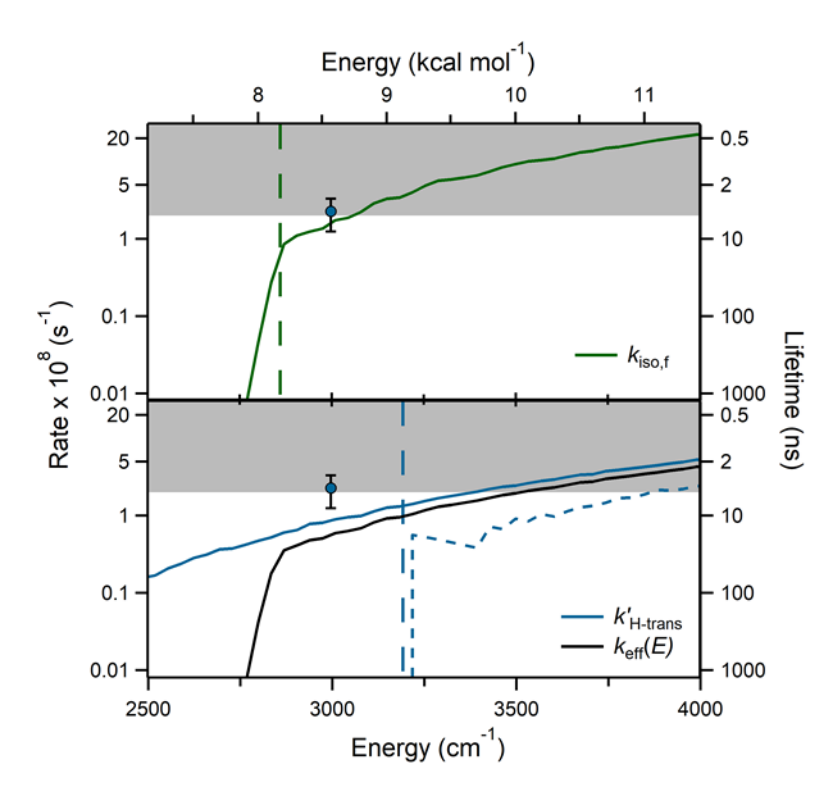


Figure 5: Experimental rate (and corresponding lifetime) with $\pm 2\sigma$ uncertainty from repeated measurements for the time-resolved appearance of OH products following IR activation of 2-butenal oxide at 2996 cm⁻¹. The rapid appearance of OH products is limited by the experimental time resolution (shaded region). RRKM calculations of the energy-dependent rates for $tZZ \rightarrow cZZ$ isomerization ($k_{\rm iso,f}$, green), modified unimolecular decay [$k'_{\rm H-trans}$, blue with (solid) and without (short dash) tunneling] that has been recast in terms of the density of states for the tZZ conformer, and effective unimolecular decay ($k_{\rm eff}(E)$, black) are shown. The torsional barrier for

internal rotation from tZZ to cZZ (green, 8.2 kcal mol⁻¹) and the effective TS barrier (blue, 9.1 kcal mol⁻¹, relative to tZZ) are indicated by vertical dashed lines.

Isomerization between tZZ and cZZ controls the effective rate below ca. 2850 cm⁻¹, while the modified rate for the 1,6 H-atom transfer process dominates above ca. 2850 cm⁻¹. Unimolecular decay to OH products occurs exclusively by tunneling below the TS barrier for 1,6 H-atom transfer at ca. 3190 cm⁻¹. As a result, quantum mechanical tunneling controls the unimolecular decay to OH products upon IR activation of the tZZ conformer at 2996 cm⁻¹.

4. Discussion

4.1 Comparison of Experimental and Theoretical Unimolecular Decay Rates

The unimolecular decay of 2-butenal oxide to OH products is shown to be remarkably rapid following fundamental CH stretch excitation at 2996 cm⁻¹, consistent with an allylic 1,6 H-atom transfer mechanism in this unsaturated Criegee intermediate. Both experiment and statistical RRKM calculations based on high level electronic structure theory indicate rapid unimolecular decay on a few nanosecond timescale. Here, we consider possible reasons for the slightly faster (4-fold) rate observed experimentally than computed theoretically, although experimental uncertainty in the rate measurement (limited by the temporal resolution of the lasers) reduces the discrepancy (2-fold) between experiment and theory.

One possible explanation stems from a broader vibrational band contour than typically observed for Criegee intermediates. An expanded view of the 2996 cm⁻¹ feature attributed to the v₄ transition of the *tZZ* conformer of 2-butenal oxide is shown in Figure S12, revealing a spectral breadth (FWHM of 13 cm⁻¹) that is significantly greater than anticipated for a single rovibrational band contour under typical jet-cooled conditions in this laboratory. The breadth of the 2996 cm⁻¹ feature could originate from several sources. One possibility is strong coupling with a nearby *tZZ* state with two quanta of excitation (Table S5). Another possibility is strong coupling to a nearby *cZZ* state that lies above the torsional barrier associated with internal rotation about the C-C bond.

Alternatively, the breadth of the 2996 cm⁻¹ feature may arise from overlapping hot band transitions originating from low frequency vibrations (δ) of the *tZZ* conformer, such as torsions or ring distortions (Table S4). Several $\delta \rightarrow \nu_4 + \delta$ hot band transitions (Table S7) are computed that could fall within the spectral breadth of the 2996 cm⁻¹ feature, if such low frequency modes are sufficiently populated. Such hot band transitions, illustrated in Figure S14, would access

higher energy vibrational states and undergo more rapid unimolecular decay than fundamental CH stretch (v_4) excitation. On the other hand, it is unlikely that direct excitation of a weak transition of the cZZ conformer (Figure 4) contributes to the experimental feature and more rapid decay since the strongest transition predicted for the cZZ conformer at 2930 cm⁻¹ is not observed.

Although high level calculations have been performed for the TS barriers associated with tZZ to cZZ isomerization and unimolecular decay of the cZZ conformer via 1,6 H-atom transfer, we nevertheless consider possible uncertainties on the predicted rates. A sensitivity analysis has been performed to evaluate the impact of reasonable estimates of the uncertainty in the computed TS barrier heights and imaginary frequencies on the RRKM rates predicted for unimolecular decay of 2-butenal oxide to OH products. Specifically, the TS barriers for isomerization and H-atom transfer are varied by ± 0.5 kcal mol⁻¹, while the imaginary frequencies are changed by $\pm 20i$ cm⁻¹ for isomerization and $\pm 200i$ cm⁻¹ for H-atom transfer in Figure S15. Since a decrease in the TS barrier height makes the greatest impact, we considered the combined change of lowering $k_{\rm iso,f}$ and $k'_{\rm H-trans}$ by 0.5 kcal mol⁻¹ on $k_{\rm eff}(E)$ in Figure S16. The combined change would bring the computed rate ($k_{\rm eff}(E) = 1.4 \times 10^8 \text{ s}^{-1}$) at 2996 cm⁻¹ into agreement with the experimental rate ($k \ge 2.3 \pm 1.0 \times 10^8 \text{ s}^{-1}$) within its $\pm 2\sigma$ uncertainty. We note that reaction-path curvature is not taken into account in the Eckart model, which could further increase the calculated tunneling contribution.⁶⁵

4.2 Comparison with Prior Studies of 1,4 H-Atom Transfer

The present study on 2-butenal oxide is the first demonstration of rapid 1,6 H-atom transfer and unimolecular decay of a Criegee intermediate. The mechanism involves isomerization from a lower (*tZZ*) to higher (*cZZ*) energy conformer, followed by 1,6 H-atom transfer and release of OH products. Prior studies have shown that higher energy conformers can contribute to OH production from Criegee intermediates *via* 1,4 H-atom transfer mechanisms. Specifically, unimolecular decay pathways for ethyl- and methyl-ethyl-substituted Criegee intermediates have been identified from higher energy conformers (CH₃CH₂CHOO: ca. 0.4 kcal mol⁻¹ and *anti*-(CH₃)(CH₃CH₂)COO (MECI2): 0.2 kcal mol⁻¹).^{20,58} For each of these Criegee intermediates, the torsional barrier (ca. 2.3 kcal mol⁻¹) separating the conformers is significantly lower than the TS barrier (ca. 16 kcal mol⁻¹) associated with 1,4 H-atom transfer and release of OH products; hence, the latter is clearly the rate limiting step. In the prior studies, the IR spectral features of the lower and higher energy conformers were overlapping, and the two conformers were

identified by their distinct unimolecular rates. In the present study on 2-butenal oxide, the lower energy tZZ conformer is identified spectroscopically and unimolecular decay proceeds via the higher energy cZZ conformer.

Further insights on the rates for unimolecular decay of Criegee intermediates can be obtained by comparing the reaction coordinates for the 1,4 and 1,6 H-atom transfer processes. Previously predicted TS barrier heights and imaginary frequencies associated with the 1,4 H-atom process are given in Table 1. The table also includes the barrier heights and imaginary frequencies associated with the isomerization and 1,6 H-atom processes for the tZZ and cZZ conformers of 2butenal oxide. The TS barriers and unimolecular decay rates for H-atom transfer leading to unimolecular decay of Criegee intermediates change dramatically when hydrogen transfer occurs via a 1,6 H-atom process rather than 1,4 H-atom shift (Table 1). For Criegee intermediates that undergo 1,4 H-atom transfer, typical TS barriers are ca. 16-18 kcal mol⁻¹. ^{18-20, 66-67} By contrast, 2-butenal oxide has a TS barrier of only ca. 4.8 kcal mol⁻¹ (relative to cZZ) that arises from its 7membered ring transition state with significantly less ring strain than the 5-membered ring transition state required for 1,4 H-atom transfer. By contrast, a 7-membered ring TS will be less favorable than a 5-membered ring TS from an entropy perspective, potentially slowing unimolecular decay. The imaginary frequency, corresponding to an effective change in the thickness of the barrier along the reaction coordinate, can also affect the tunneling weighted decay rate. The imaginary frequencies associated with the 1,4 H-atom transfer mechanism previously investigated range from 1710i - 1755i cm⁻¹. For 2-butenal oxide, the imaginary frequency associated with the 1,6 H-atom transfer mechanism is 1334i cm⁻¹. This decrease in imaginary frequency results in an increase in the breadth of the TS barrier, which slows tunneling and the tunneling weighted decay rate. The significant decrease in the TS barrier for 1,6 vs. 1,4 H-atom transfer causes a dramatic increase in isomerization rate, while the reduced tunneling contribution to the rate for 1,6 vs. 1,4 H-atom transfer is consistent with the lower imaginary frequency. Figure 6 compares the Eckart potentials in mass-weighted coordinates for syn-CH₃CHOO (black) and 2-butenal oxide (blue) to isomerization products via 1,4 and 1,6 Hatom transfer processes, respectively. Changes in the TS barrier, height and width are evident. Overall, the significant change in barrier height is the dominant factor resulting in very rapid unimolecular decay rates for 2-butenal oxide via 1,6 H-atom transfer. The Eckart potentials for

unimolecular decay of other Criegee intermediates *via* 1,4 H-atom transfer (Figure S17) are similar to that of *syn*-CH₃CHOO.

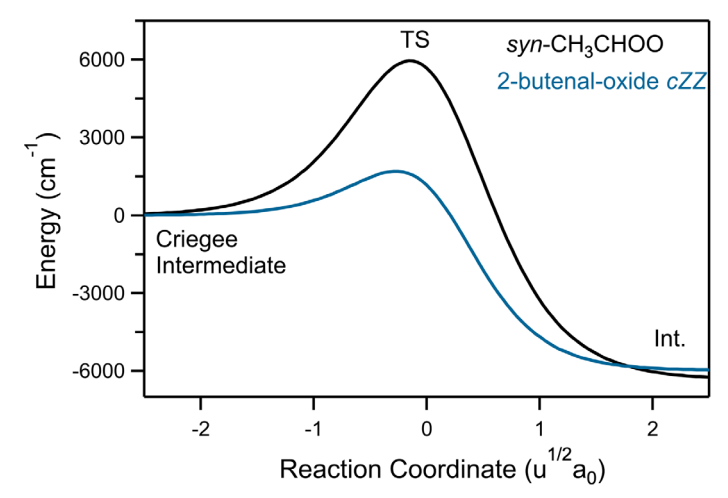


Figure 6: Eckart potentials in mass-weighed coordinates [reduced mass (u) and distance (a₀)] for 1,4 H-atom transfer from *syn*-CH₃CHOO to vinyl hydroperoxide (black) and 1,6 H-atom transfer from 2-butenal oxide to (*E*)-1-hydroperoxybuta-1,3-diene (blue).

Table 1: Calculated transition state (TS) barrier heights and imaginary frequencies associated with the 1,4 and 1,6 H-atom transfer processes for a series of Criegee intermediates. TS barriers are calculated with the ANL0-B2F level of theory, while anharmonic frequencies are obtained with the B2PLYP-D3/cc-pVTZ level of theory.

Criegee intermediate	TS barrier	Frequency
	[kcal mol ⁻¹]	[cm ⁻¹]
H-atom transfer		
syn-CH ₃ CHOO	17.05^{a}	1734 <i>i</i> ^b
syn-CH ₃ CH ₂ CHOO	16.46 ^c	1724 <i>i</i> ^b
anti-MECI ^d	16.14	1719i
syn-MECI ^d	15.41	1724 <i>i</i>
(CH ₃) ₂ COO	16.16 ^a	1709 <i>i</i> ^b
syn-MVK-oxide ^e	18.00	1755 <i>i</i>
2-butenal oxide (<i>cZZ</i>)	4.87	1334 <i>i</i>
Isomerization		
tZZ to cZZ	8.12	119 <i>i</i>

a. Ref. 18.

b. Recalculated in the present study; see Refs. 18, 53 for prior calculations.

c. Ref. 58.

d. Methyl-ethyl substituted Criegee intermediate (MECI); Ref. 20.

e. Methyl vinyl ketone oxide (MVK-oxide) Criegee intermediate; Ref. 16.

Master equation modeling has also been utilized to extend the energy-dependent unimolecular decay rates $k_{\rm eff}(E)$ for 2-butenal oxide to thermal conditions. The thermal rate predicted at 298 K, 1 bar for (1) the combined isomerization from tZZ to cZZ and unimolecular decay from cZZ to OH products via the 1,6 H-atom transfer process and (2) direct unimolecular decay of tZZ to OH products is exceedingly fast at 8×10^5 s⁻¹, as shown in Figure 7 (and Table S12). This is over 3 orders of magnitude faster than the thermal decay rates predicted and/or directly measured for CH₃CHOO and (CH₃)₂COO via 1,4 H-atom transfer that range from 120 to 370 s⁻¹ at 298 K.^{16-17, 58, 66, 68-71} It is 4 orders of magnitude faster than the corresponding thermal rate predicted for MVK-oxide via 1,4 H-atom transfer of 33 s⁻¹.¹⁶

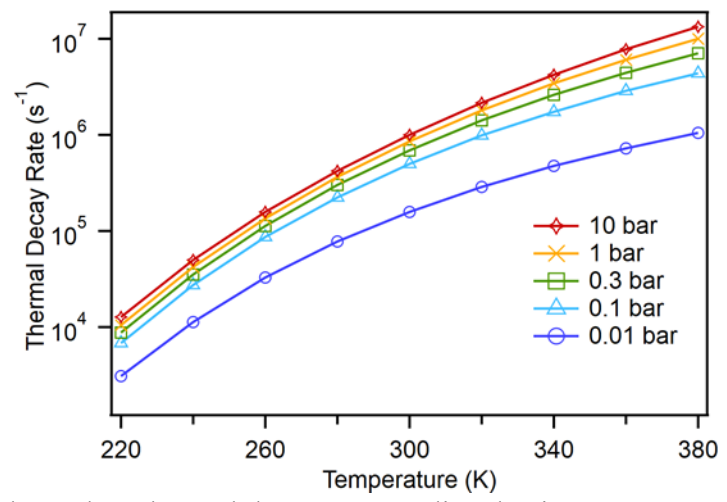


Figure 7: Pressure-dependent thermal decay rate predicted using master equation modeling for tZZ and cZZ conformers of 2-butenal oxide from 220 to 380 K. The thermal decay rate results from the combined isomerization from tZZ to cZZ and unimolecular decay from cZZ to OH products as well as direct unimolecular decay of tZZ to OH products.

5. Conclusion

A novel four carbon Criegee intermediate, 2-butenal oxide, has been generated from a newly synthesized precursor and directly detected using IR action spectroscopy. Unique to the 2-butenal oxide Criegee intermediate is extended conjugation across the unsaturated carbon chain and carbonyl oxide functional groups that facilitates rapid allylic 1,6 H-atom transfer. A lowenergy (*tZZ*) conformer is shown to isomerize to a higher energy (*cZZ*) conformer that undergoes unimolecular decay *via* 1,6 H-atom transfer and yields OH products. The isomerization and unimolecular decay are initiated by IR activation in the fundamental CH stretching region and detected by UV LIF of the resultant OH products. This protocol yields an IR spectral signature for the *tZZ* conformer of 2-butenal oxide with a strong feature at 2996 cm⁻¹, along with weaker

and less distinctive features from 2900 to 3150 cm⁻¹. Overall, the experimental IR action spectrum agrees well with the theoretically predicted IR absorption spectrum (VPT2). The rate of appearance of OH products following IR activation of the tZZ conformer at 2996 cm⁻¹ is ≥ 2.3 $\pm 1.0 \times 10^8$ s⁻¹, which is within the experimental time resolution. A kinetic model is developed that involves isomerization between the tZZ and cZZ conformers and unimolecular decay to OH products via 1,6 H-atom transfer through a 7-membered ring transition state. The theoretically predicted decay rates are in good agreement with the rapid decay observed experimentally. The unimolecular decay of 2-butenal oxide via the allylic 1,6 H-transfer process is significantly faster than the typical alkyl 1,4 H-atom transfer mechanism, i.e. three orders of magnitude faster than that obtained for syn-CH₃CHOO at a similar energy. ¹⁸ This change in rate is mainly caused by a significant decrease in the TS barrier from ca. 16 – 18 kcal mol⁻¹ for 1,4 H-atom transfer to ca. 5 kcal mol⁻¹ associated with 1,6 H-atom transfer of the cZZ conformer of 2-butenal oxide. Moreover, the thermal decay rate predicted for 2-butenal oxide at 298 K, 1 bar is exceedingly fast at ca. 10⁶ s⁻¹. Overall, this combined experimental and theoretical study of 2-butenal oxide reveals rapid allylic 1,6 H-atom transfer for the unimolecular decay of a Criegee intermediate for the first time.

ASSOCIATED CONTENT

Supporting Information

The Supporting Information contains additional details on synthetic, experimental and theoretical methods; experimental and computed IR spectral properties, temporal profiles; and unimolecular decay rates.

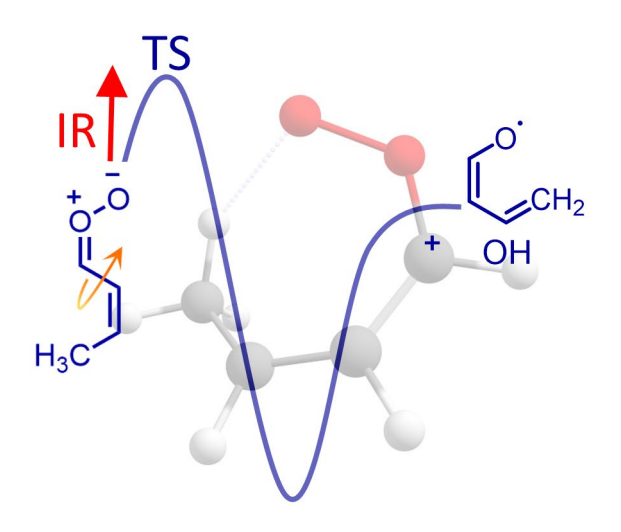
Data Availability

The data that support the findings of this study are available within the article and its supporting information. In addition, the MESS input files and optimized geometries are provided in Zenodo (Ref. 72), while other supplementary information is presented in the Corrigendum (Ref. 32).

Acknowledgments

The spectroscopic investigation was primarily supported by the National Science Foundation under grant CHE-1955068 (MIL). This work utilized the Extreme Science and Engineering Discovery Environment (XSEDE), which is supported by the National Science Foundation grant number ACI-1548562 through the allocation TG-CHE190088. ASH gratefully acknowledges support from the Carlsberg Foundation (CF18–0614) and the Independent Research Fund

Denmark (9036–00016B). MCK is grateful to the NSF (CHE 2102626) for financial support of this research. Partial instrumentation support for the MCK laboratory was provided by the NIH (1S10RR023444, 1S10RR022442, 3R01GM118510-03S1, 3R01GM087605-06S1). The contributions from SJK were supported by the U.S. Department of Energy (USDOE), Office of Basic Energy Sciences, Division of Chemical Sciences, Geosciences, and Biosciences under DOE Contract Number DE-AC02-06CH11357. This material is also based upon work supported by the National Science Foundation Graduate Research Fellowship Program under Grant No. DGE-1845298 (VJE). The authors thank Tianlin Liu and Meijun Zou for recording the time-of-flight data.



TOC figure

References

- 1. Sindelarova, K.; Granier, C.; Bouarar, I.; Guenther, A.; Tilmes, S.; Stavrakou, T.; Müller, J. F.; Kuhn, U.; Stefani, P.; Knorr, W., Global data set of biogenic VOC emissions calculated by the MEGAN model over the last 30 years. *Atmos. Chem. Phys.* **2014**, *14* (17), 9317-9341.
- 2. Harrison, R. M.; Yin, J.; Tilling, R. M.; Cai, X.; Seakins, P. W.; Hopkins, J. R.; Lansley, D. L.; Lewis, A. C.; Hunter, M. C.; Heard, D. E.; Carpenter, L. J.; Creasey, D. J.; Lee, J. D.; Pilling, M. J.; Carslaw, N.; Emmerson, K. M.; Redington, A.; Derwent, R. G.; Ryall, D.; Mills, G.; Penkett, S. A., Measurement and modelling of air pollution and atmospheric chemistry in the U.K. West Midlands conurbation: Overview of the PUMA consortium project. *Sci. Total Environ.* **2006**, *360* (1–3), 5-25.
- 3. Elshorbany, Y. F.; Kurtenbach, R.; Wiesen, P.; Lissi, E.; Rubio, M.; Villena, G.; Gramsch, E.; Rickard, A. R.; Pilling, M. J.; Kleffmann, J., Oxidation capacity of the city air of Santiago, Chile. *Atmos. Chem. Phys.* **2009**, *9* (6), 2257-2273.
- 4. Emmerson, K. M.; Carslaw, N.; Carslaw, D. C.; Lee, J. D.; McFiggans, G.; Bloss, W. J.; Gravestock, T.; Heard, D. E.; Hopkins, J.; Ingham, T.; Pilling, M. J.; Smith, S. C.; Jacob, M.; Monks, P. S., Free radical modelling studies during the UK TORCH campaign in summer 2003. *Atmos. Chem. Phys.* **2007**, *7* (1), 167-181.
- 5. Taatjes, C. A.; Shallcross, D. E.; Percival, C. J., Research frontiers in the chemistry of Criegee intermediates and tropospheric ozonolysis. *Phys. Chem. Chem. Phys.* **2014**, *16* (5), 1704-1718.
- 6. Khan, M. A. H.; Percival, C. J.; Caravan, R. L.; Taatjes, C. A.; Shallcross, D. E., Criegee intermediates and their impacts on the troposphere. *Environ Sci-Proc. Imp.* **2018**, *20* (3), 437-453.
- 7. Johnson, D.; Marston, G., The gas-phase ozonolysis of unsaturated volatile organic compounds in the troposphere. *Chem. Soc. Rev.* **2008**, *37* (4), 699-716.
- 8. Pfeifle, M.; Ma, Y.-T.; Jasper, A. W.; Harding, L. B.; Hase, W. L.; Klippenstein, S. J., Nascent energy distribution of the Criegee intermediate CH2OO from direct dynamics calculations of primary ozonide dissociation. *J. Chem. Phys.* **2018**, *148* (17), 174306.
- 9. Vereecken, L.; Novelli, A.; Taraborrelli, D., Unimolecular decay strongly limits the atmospheric impact of Criegee intermediates. *Phys. Chem. Chem. Phys.* **2017**, *19* (47), 31599-31612.
- 10. Stephenson, T. A.; Lester, M. I., Unimolecular decay dynamics of Criegee intermediates: Energy-resolved rates, thermal rates, and their atmospheric impact. *Int. Rev. Phys. Chem.* **2020**, *39* (1), 1-33.
- 11. Donahue, N. M.; Drozd, G. T.; Epstein, S. A.; Presto, A. A.; Kroll, J. H., Adventures in ozoneland: Down the rabbit-hole. *Phys. Chem. Chem. Phys.* **2011**, *13* (23), 10848-10857.
- 12. Vereecken, L.; Francisco, J. S., Theoretical studies of atmospheric reaction mechanisms in the troposphere. *Chem. Soc. Rev.* **2012**, *41* (19), 6259-6293.
- 13. Liu, F.; Beames, J. M.; Petit, A. S.; McCoy, A. B.; Lester, M. I., Infrared-driven unimolecular reaction of CH₃CHOO Criegee intermediates to OH radical products. *Science* **2014**, *345* (6204), 1596-1598.
- 14. Liu, F.; Beames, J. M.; Lester, M. I., Direct production of OH radicals upon CH overtone activation of (CH₃)₂COO Criegee intermediates. *J. Chem. Phys.* **2014**, *141* (23), 234312.
- 15. Lester, M. I.; Klippenstein, S. J., Unimolecular Decay of Criegee Intermediates to OH Radical Products: Prompt and Thermal Decay Processes. *Acc. Chem. Res.* **2018**, *51* (4), 978-985.
- 16. Barber, V. P.; Pandit, S.; Green, A. M.; Trongsiriwat, N.; Walsh, P. J.; Klippenstein, S. J.; Lester, M. I., Four-carbon Criegee intermediate from isoprene ozonolysis: Methyl vinyl ketone oxide synthesis, infrared spectrum, and OH production. *J. Am. Chem. Soc.* **2018**, *140* (34), 10866-10880.
- 17. Fang, Y.; Liu, F.; Barber, V. P.; Klippenstein, S. J.; McCoy, A. B.; Lester, M. I., Deep tunneling in the unimolecular decay of CH₃CHOO Criegee intermediates to OH radical products. *J. Chem. Phys.* **2016**, *145* (23), 234308.
- 18. Fang, Y.; Liu, F.; Barber, V. P.; Klippenstein, S. J.; McCoy, A. B.; Lester, M. I., Communication: Real time observation of unimolecular decay of Criegee intermediates to OH radical products. *J. Chem. Phys.* **2016**, *144* (6), 061102.

- 19. Fang, Y.; Barber, V. P.; Klippenstein, S. J.; McCoy, A. B.; Lester, M. I., Tunneling effects in the unimolecular decay of (CH₃)₂COO Criegee intermediates to OH radical products. *J. Chem. Phys.* **2017**, *146* (13), 134307.
- 20. Barber, V. P.; Hansen, A. S.; Georgievskii, Y.; Klippenstein, S. J.; Lester, M. I., Experimental and theoretical studies of the double-substituted methyl ethyl Criegee intermediate: Infrared action spectroscopy and unimolecular decay to OH radical products. *J. Chem. Phys.* **2020**, *152*, 094301.
- 21. Welz, O.; Savee, J. D.; Osborn, D. L.; Vasu, S. S.; Percival, C. J.; Shallcross, D. E.; Taatjes, C. A., Direct kinetic measurements of Criegee intermediate (CH₂OO) formed by reaction of CH₂I with O₂. *Science* **2012**, *335* (6065), 204-207.
- 22. Taatjes, C. A.; Welz, O.; Eskola, A. J.; Savee, J. D.; Scheer, A. M.; Shallcross, D. E.; Rotavera, B.; Lee, E. P. F.; Dyke, J. M.; Mok, D. K. W.; Osborn, D. L.; Percival, C. J., Direct measurements of conformer-dependent reactivity of the Criegee intermediate CH₃CHOO. *Science* **2013**, *340* (6129), 177-180.
- 23. Barber, V. P.; Pandit, S.; Esposito, V. J.; McCoy, A. B.; Lester, M. I., CH stretch activation of CH₃CHOO: Deep tunneling to hydroxyl radical products. *J. Phys. Chem. A* **2019**, *123* (13), 2559-2569.
- 24. Stone, D.; Au, K.; Sime, S.; Medeiros, D. J.; Blitz, M.; Seakins, P. W.; Decker, Z.; Sheps, L., Unimolecular decomposition kinetics of the stabilised Criegee intermediates CH₂OO and CD₂OO. *Phys. Chem. Chem. Phys.* **2018**, *20* (38), 24940-24954.
- 25. Vereecken, L.; Novelli, A.; Kiendler-Scharr, A.; Wahner, A., Reactions of oxygenated and unsaturated Criegee intermediates under atmospheric conditions. *Phys. Chem. Chem. Phys.* **2022**, Advance Article. DOI: 10.1039/D1CP05877K.
- 26. Vereecken, L.; Peeters, J., A structure–activity relationship for the rate coefficient of H-migration in substituted alkoxy radicals. *Phys. Chem. Chem. Phys.* **2010**, *12* (39), 12608-12620.
- 27. Davis, A. C.; Francisco, J. S., Reactivity trends within alkoxy radical reactions responsible for chain branching. *J. Am. Chem. Soc.* **2011**, *133* (45), 18208-18219.
- 28. Otkjær, R. V.; Jakobsen, H. H.; Tram, C. M.; Kjaergaard, H. G., Calculated hydrogen shift rate constants in substituted alkyl peroxy radicals. *J. Phys. Chem. A* **2018**, *122* (43), 8665-8673.
- 29. Vereecken, L.; Nozière, B., H migration in peroxy radicals under atmospheric conditions. *Atmos. Chem. Phys.* **2020**, *20* (12), 7429-7458.
- 30. Tao, H.; Lin, K. C., Kinetic barriers, rate constants and branching ratios for unimolecular reactions of methyl octanoate peroxy radicals: A computational study of a mid-sized biodiesel fuel surrogate. *Combust. Flame* **2017**, *180*, 148-157.
- 31. Lewin, A. G.; Johnson, D.; Price, D. W.; Marston, G., Aspects of the kinetics and mechanism of the gas-phase reactions of ozone with conjugated dienes. *Phys. Chem. Chem. Phys.* **2001**, *3* (7), 1253-1261.
- 32. Vereecken, L., "Corrigendum supporting information Vereecken et al. 2017", https://doi.org/10.26165/JUELICH-DATA/UJ8OUQ. V1 ed.; Jülich DATA: 2021.
- 33. Vansco, M. F.; Marchetti, B.; Trongsiriwat, N.; Wang, G.; Bhagde, T.; Walsh, P. J.; Klippenstein, S. J.; Lester, M. I., Synthesis, electronic spectroscopy and photochemistry of methacrolein oxide: A four carbon unsaturated Criegee intermediate from isoprene ozonolysis. *J. Am. Chem. Soc.* **2019**, *141*, 15058-15069.
- 34. Vansco, M. F.; Caravan, R. L.; Zuraski, K.; Winiberg, F. A. F.; Au, K.; Trongsiriwat, N.; Walsh, P. J.; Osborn, D. L.; Percival, C. J.; Taatjes, C. A.; Lester, M. I., Experimental evidence of dioxole unimolecular decay pathway for isoprene-derived Criegee intermediates. *J. Phys. Chem. A* **2020**, *124*, 3542-3554.
- 35. Beames, J. M.; Liu, F.; Lu, L.; Lester, M. I., Ultraviolet spectrum and photochemistry of the simplest Criegee intermediate CH₂OO. *J. Am. Chem. Soc.* **2012**, *134* (49), 20045-20048.
- 36. Beames, J. M.; Liu, F.; Lu, L.; Lester, M. I., UV spectroscopic characterization of an alkyl substituted Criegee intermediate CH₃CHOO. *J. Chem. Phys.* **2013**, *138* (24), 244307.

- 37. Sheps, L.; Scully, A. M.; Au, K., UV absorption probing of the conformer-dependent reactivity of a Criegee intermediate CH₃CHOO. *Phys. Chem. Chem. Phys.* **2014**, *16* (48), 26701-26706.
- 38. Chang, Y.-P.; Chang, C.-H.; Takahashi, K.; Lin, J. J.-M., Absolute UV absorption cross sections of dimethyl substituted Criegee intermediate (CH₃)₂COO. *Chem. Phys. Lett.* **2016**, *653*, 155-160.
- 39. Liu, F.; Beames, J. M.; Green, A. M.; Lester, M. I., UV spectroscopic characterization of dimethyland ethyl-substituted carbonyl oxides. *J. Phys. Chem. A* **2014**, *118* (12), 2298-2306.
- 40. Cabezas, C.; Guillemin, J.-C.; Endo, Y., Probing the conformational behavior of the doubly substituted methyl-ethyl Criegee intermediate by FTMW spectroscopy. *J. Chem. Phys.* **2017**, *146* (17), 174304.
- 41. Vansco, M. F.; Marchetti, B.; Lester, M. I., Electronic spectroscopy of methyl vinyl ketone oxide: A four-carbon unsaturated Criegee intermediate from isoprene ozonolysis. *J. Chem. Phys.* **2018**, *149* (24), 244309.
- 42. Manickam, G.; Siddappa, U.; Li, Y., Selective one-pot synthesis of Z-iodoallylic iodides from propargyl alcohols. *Tetrahedron Lett.* **2006**, *47* (33), 5867-5868.
- 43. Gras, J.-L.; Chang, Y. Y. K. W.; Bertrand, M., Sur la réaction de l'iodure de triméthylsilyle avec les alcools acétyléniques. *Tetrahedron Lett.* **1982**, *23* (35), 3571-3572.
- 44. Chen, V. Y.; Kwon, O., Unified approach to furan natural products via phosphine-palladium catalysis. *Angew. Chemie Int. Ed.* **2021**, *60* (16), 8874-8881.
- 45. Klippenstein, S. J.; Harding, L. B.; Ruscic, B., Ab initio computations and active thermochemical tables hand in hand: Heats of formation of core combustion species. *J. Phys. Chem. A* **2017**, *121* (35), 6580-6602.
- 46. Grimme, S.; Ehrlich, S.; Goerigk, L., Effect of the damping function in dispersion corrected density functional theory. *J. Comput. Chem.* **2011**, *32* (7), 1456-1465.
- 47. Werner, H.-J.; Knowles, P. J.; Knizia, G.; Manby, F. R.; Schütz, M., Molpro: A general-purpose quantum chemistry program package. *WIREs Computational Molecular Science* **2012**, *2* (2), 242-253.
- 48. Werner, H.-J.; Knowles, P. J.; Knizia, G.; Manby, F. R.; Schütz, M.; Celani, P.; Györffy, W.; Kats, D.; Korona, T.; Lindh, R.; Mitrushenkov, A.; Rauhut, G.; Shamasundar, K. R.; Adler, T. B.; Amos, R. D.; Bernhardsson, A.; Berning, A.; Cooper, D. L.; Deegan, M. J. O.; Dobbyn, A. J.; Eckert, F.; Goll, E.; Hampel, C.; Hesselmann, A.; Hetzer, G.; Hrenar, T.; Jansen, G.; Köppl, C.; Liu, Y.; Lloyd, A. W.; Mata, R. A.; May, A. J.; McNicholas, S. J.; Meyer, W.; Mura, M. E.; Nicklaß, A.; O'Neill, D. P.; Palmieri, P.; Peng, D.; Pflüger, K.; Pitzer, R.; Reiher, M.; Shiozaki, T.; Stoll, H.; Stone, A. J.; Tarroni, R.; Thorsteinsson, T.; Wang, M.; Welborn, M., MOLPRO 2019.1, a package of *ab initio* programs, see www.molpro.net. 2019.
- 49. Matthews, D. A.; Cheng, L.; Harding, M. E.; Lipparini, F.; Stopkowicz, S.; Jagau, T.-C.; Szalay, P. G.; Gauss, J.; Stanton, J. F., Coupled-cluster techniques for computational chemistry: The CFOUR program package. *J. Chem. Phys.* **2020**, *152* (21), 214108.
- 50. Stanton, J. F.; Gauss, J.; Cheng, L.; Harding, M. E.; Matthews, D. A.; Szalay, P. G., CFOUR, Coupled-Cluster techniques for Computational Chemistry, a quantum-chemical program package.
- 51. Frisch, M. J.; Trucks, G. W.; Schlegel, H. B.; Scuseria, G. E.; Robb, M. A.; Cheeseman, J. R.; Scalmani, G.; Barone, V.; Petersson, G. A.; Nakatsuji, H.; Li, X.; Caricato, M.; Marenich, A. V.; Bloino, J.; Janesko, B. G.; Gomperts, R.; Mennucci, B.; Hratchian, H. P.; Ortiz, J. V.; Izmaylov, A. F.; Sonnenberg, J. L.; Williams-Young, D.; Ding, F.; Lipparini, F.; Egidi, F.; Goings, J.; Peng, B.; Petrone, A.; Henderson, T.; Ranasinghe, D.; Zakrzewski, V. G.; Gao, J.; Rega, N.; Zheng, G.; Liang, W.; Hada, M.; Ehara, M.; Toyota, K.; Fukuda, R.; Hasegawa, J.; Ishida, M.; Nakajima, T.; Honda, Y.; Kitao, O.; Nakai, H.; Vreven, T.; Throssell, K.; Montgomery, J. J. A.; Peralta, J. E.; Ogliaro, F.; Bearpark, M. J.; Heyd, J. J.; Brothers, E. N.; Kudin, K. N.; Staroverov, V. N.; Keith, T. A.; Kobayashi, R.; Normand, J.; Raghavachari, K.; Rendell, A. P.; Burant, J. C.; Iyengar, S. S.; Tomasi, J.; Cossi, M.; Millam, J. M.; Klene, M.; Adamo, C.; Cammi, R.; Ochterski, J. W.; Martin, R. L.; Morokuma, K.; Farkas, O.; Foresman, J. B.; Fox, D. J. Gaussian 16 Rev. A.03, Wallingford CT Wallingford, CT, 2016.
- 52. Nielsen, H. H., The Vibration-Rotation Energies of Molecules. Rev. Mod. Phys. 1951, 23 (2), 90-136.

- 53. Kuhler, K. M.; Truhlar, D. G.; Isaacson, A. D., General method for removing resonance singularities in quantum mechanical perturbation theory. *J. Chem. Phys.* **1996**, *104* (12), 4664-4671.
- 54. Bloino, J.; Biczysko, M.; Barone, V., General Perturbative Approach for Spectroscopy, Thermodynamics, and Kinetics: Methodological Background and Benchmark Studies. *J. Chem. Theory Comput.* **2012**, *8* (3), 1015-1036.
- 55. Towns, J.; Cockerill, T.; Dahan, M.; Foster, I.; Gaither, K.; Grimshaw, A.; Hazlewood, V.; Lathrop, S.; Lifka, D.; Peterson, G. D.; Roskies, R.; Scott, J. R.; Wilkens-Diehr, N., XSEDE: Accelerating scientific discovery. *Comput. Sci. Eng.* **2014**, *16* (5), 62-74.
- 56. Baer, T.; Hase, W. L., *Unimolecular reaction dynamics theory and experiments*. Oxford University Press: New York, 1996.
- 57. Georgievskii, Y.; Klippenstein, S. J., *MESS, MESS Master Equation System Solver*, https://github.com/Auto-Mech/MESS (accessed 2021-04-24).
- 58. Fang, Y.; Liu, F.; Klippenstein, S. J.; Lester, M. I., Direct observation of unimolecular decay of CH₃CH₂CHOO Criegee intermediates to OH radical products. *J. Chem. Phys.* **2016**, *145* (4), 044312.
- 59. Hewett, D. M.; Bocklitz, S.; Tabor, D. P.; Sibert III, E. L.; Suhm, M. A.; Zwier, T. S., Identifying the first folded alkylbenzene via ultraviolet, infrared, and Raman spectroscopy of pentylbenzene through decylbenzene. *Chem. Sci.* **2017**, *8* (8), 5305-5318.
- 60. Korn, J. A.; Tabor, D. P.; Sibert III, E. L.; Zwier, T. S., Conformation-specific spectroscopy of alkyl benzyl radicals: Effects of a radical center on the CH stretch infrared spectrum of an alkyl chain. *J. Chem. Phys.* **2016**, *145* (12), 124314.
- 61. Tabor, D. P.; Hewett, D. M.; Bocklitz, S.; Korn, J. A.; Tomaine, A. J.; Ghosh, A. K.; Zwier, T. S.; Sibert III, E. L., Anharmonic modeling of the conformation-specific IR spectra of ethyl, n-propyl, and n-butylbenzene. *J. Chem. Phys.* **2016**, *144* (22), 224310.
- 62. Green, A. M.; Barber, V. P.; Fang, Y.; Klippenstein, S. J.; Lester, M. I., Selective deuteration illuminates the importance of tunneling in the unimolecular decay of Criegee intermediates to hydroxyl radical products. *Proc. Natl. Acad. Sci.* **2017**, *114* (47), 12372-12377.
- 63. Hansen, A. S.; Bhagde, T.; Moore, K. B.; Moberg, D. R.; Jasper, A. W.; Georgievskii, Y.; Vansco, M. F.; Klippenstein, S. J.; Lester, M. I., Watching a hydroperoxyalkyl radical (•QOOH) dissociate. *Science* **2021**, *373* (6555), 679-682.
- 64. Georgievskii, Y.; Miller, J. A.; Burke, M. P.; Klippenstein, S. J., Reformulation and solution of the master equation for multiple-well chemical reactions. *J. Phys. Chem. A* **2013**, *117* (46), 12146-12154.
- 65. Bao, J. L.; Truhlar, D. G., Variational transition state theory: theoretical framework and recent developments. *Chem. Soc. Rev.* **2017**, *46* (24), 7548-7596.
- 66. Long, B.; Bao, J. L.; Truhlar, D. G., Atmospheric Chemistry of Criegee Intermediates: Unimolecular Reactions and Reactions with Water. *J. Am. Chem. Soc.* **2016**, *138* (43), 14409-14422.
- 67. Long, B.; Bao, J. L.; Truhlar, D. G., Unimolecular reaction of acetone oxide and its reaction with water in the atmosphere. *Proc. Natl. Acad. Sci. U.S.A.* **2018**, *115* (24), 6135-6140.
- 68. Zhou, X.; Liu, Y.; Dong, W.; Yang, X., Unimolecular Reaction Rate Measurement of *syn*-CH₃CHOO. *J. Phys. Chem. Lett.* **2019**, *10* (17), 4817-4821.
- 69. Nguyen, T. L.; McCaslin, L.; McCarthy, M. C.; Stanton, J. F., Communication: Thermal unimolecular decomposition of *syn*-CH₃CHOO: A kinetic study. *J. Chem. Phys.* **2016**, *145* (13), 131102.
- 70. Smith, M. C.; Chao, W.; Takahashi, K.; Boering, K. A.; Lin, J. J.-M., Unimolecular decomposition rate of the Criegee intermediate (CH₃)₂COO measured directly with UV absorption spectroscopy. *J. Phys. Chem. A* **2016**, *120* (27), 4789–4798.
- 71. Chhantyal-Pun, R.; Welz, O.; Savee, J. D.; Eskola, A. J.; Lee, E. P. F.; Blacker, L.; Hill, H. R.; Ashcroft, M.; Khan, M. A. H.; Lloyd-Jones, G. C.; Evans, L.; Rotavera, B.; Huang, H.; Osborn, D. L.; Mok, D. K. W.; Dyke, J. M.; Shallcross, D. E.; Percival, C. J.; Orr-Ewing, A. J.; Taatjes, C. A., Direct measurements of unimolecular and bimolecular reaction kinetics of the Criegee intermediate (CH₃)₂COO. *J. Phys. Chem. A* **2017**, *121* (1), 4-15.
- 72. Hansen, A. S.; Qian, Y.; Sojdak, C. A.; Kozlowski, M.; Esposito, V. J.; Francisco, J. S.; Klippenstein, S. J.; Lester, M. I., Zenodo, https://doi.org/10.5281/zenodo.6323758, **2021**.